Research Article Vol. 2, No. 10 / October 2015 / Optica 912

High-resolution single-shot spectral monitoring of hard x-ray free-electron laser radiation

M. Makita,[1,*] P. Karvinen,[1,4] D. Zhu,[2] P. N. Juranic,[1] J. Grünert,[3] S. Cartier,[1] J. H. Jungmann-Smith,[1] H. T. Lemke,[2] A. Mozzanica,[1] S. Nelson,[2] L. Patthey,[1] M. Sikorski,[2] S. Song,[2] Y. Feng,[2] and C. David[1]

[1]Paul Scherrer Institut, CH 5232 Villigen-PSI, Switzerland
[2]Linac Coherent Light Source, SLAC National Accelerator Laboratory, Menlo Park, California 94025, USA
[3]European XFEL GmbH, D 22607 Hamburg, Germany
[4]Currently at: Finnlitho Ltd, FI-80140 Joensuu, Finland
*Corresponding author: mikako.makita@psi.ch

Received 8 July 2015; revised 8 September 2015; accepted 8 September 2015 (Doc. ID 245349); published 16 October 2015

We have developed an on-line spectrometer for hard x-ray free-electron laser (XFEL) radiation based on a nanostructured diamond diffraction grating and a bent crystal analyzer. Our method provides high spectral resolution, interferes negligibly with the XFEL beam, and can withstand the intense hard x-ray pulses at high repetition rates of >100 Hz. The spectrometer is capable of providing shot-to-shot spectral information for the normalization of data obtained in scientific experiments and optimization of the accelerator operation parameters. We have demonstrated these capabilities of the setup at the Linac Coherent Light Source, in self-amplified spontaneous emission mode at full energy of >1 mJ with a 120 Hz repetition rate, obtaining a resolving power of $E/\delta E > 3 \times 10^4$. The device was also used to monitor the effects of pulse duration down to 8 fs by analysis of the spectral spike width.

OCIS codes: (050.1950) Diffraction gratings; (120.6200) Spectrometers and spectroscopic instrumentation; (120.4290) Nondestructive testing; (120.4570) Optical design of instruments; (340.7480) X-rays, soft x-rays, extreme ultraviolet (EUV).

http://dx.doi.org/10.1364/OPTICA.2.000912

1. INTRODUCTION

Self-amplified spontaneous emission (SASE) is currently the most common method for the generation of short radiation pulses at x-ray free-electron laser (XFEL) facilities. Due to its stochastic nature, the pulses produced fluctuate both in intensity and in spectral composition [1,2]. These fluctuations can affect the interpretation of the measurements performed at XFEL facilities. An *in situ* diagnostics tool that provides well-resolved spectral measurements of each individual pulse without compromising the quality of the beam delivered to the experiment is needed to mitigate the effects of these fluctuations on experimental results.

Several technical approaches have been pursued to this end, for example, single-shot spectral measurements of the SASE pulses in the soft x-ray range [3–5]. For the hard x-ray range, a method using a focusing mirror to create a divergent x-ray beam and a flat silicon crystal for spectral dispersion [Fig. 1(a)] was demonstrated and implemented at the SPring-8 Ångstrom Compact Free Electron Laser (SACLA) in Japan [6–8]. Although this technique provides highly resolved spectra, it is invasive such that the beam cannot be used for experiments after passing the mirror. More recently, two independent techniques in the hard x-ray range were tested at Linac Coherent Light Source (LCLS): one that used bent Bragg diffraction crystals [Fig. 1(b)] [9] and one based on a focusing transmission grating [Fig. 1(c)] [10]. The spectrometer based on a thin bent crystal [9] offers a high spectral resolution of better than ~0.2 eV, as well as a non-demanding alignment, but causes significant beam intensity loss of up to 50% at lower photon energies due to absorption. The grating-based method [10] has the advantages of high x-ray beam transmission and radiation hardness, but suffers from a limited spectral resolution of the order of 1.5 eV.

In this Article we present a novel single-shot on-line spectrometer for hard x-rays [Fig. 2(a)] that has the benefits of both the diffraction grating [10] and the high-resolution crystal analyzer methods [6,9], yet overcomes their respective disadvantages. The key aspect for such an achievement is to combine the noninvasive, radiation hard, and highly transmissive diffraction grating with one of the high-resolution crystal spectral analyzers [6,9].

2. METHODS

Figure 2(a) shows a schematic drawing of the setup we used, with a bent crystal analyzer [9].

A beam splitter grating of pitch d is placed in the direct x-ray beam of wavelength λ. The grating diverts a small portion of the XFEL pulse onto a bent crystal spectrometer, and transmits the rest of the pulse to be used for experimental purposes. The grating lines are placed in the vertical orientation, so that the diffracted beams are deflected in the horizontal direction. At a distance D

2334-2536/15/100912-05$15/0$15.00

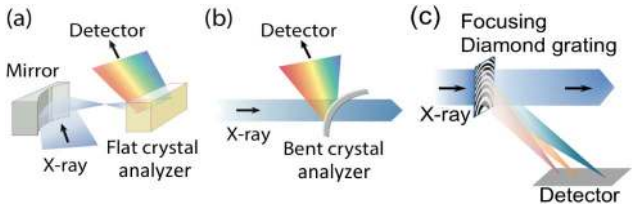

Fig. 1. Schematic drawings of the setup concepts for hard x-ray single-shot spectrometers using (a) a focusing mirror with a flat crystal analyser [6], (b) a bent crystal analyzer [9], and (c) a focusing grating [10].

downstream of the grating, the diffracted beams have a separation Δy with respect to the direct (0th-order) beam of

$$\Delta y \approx \frac{m\lambda D}{d}, \tag{1}$$

where m is the diffraction order.

In the presented setup a bent crystal analyzer spectrometer is placed in the grating's 1st-order ($m = 1$) diffracted beam for spectral monitoring. The crystal is bent convex to the incoming beam, hence different parts of the beam in the vertical direction have different incidence angles. Only the wavelength that satisfies the Bragg condition at a certain part of the crystal will be diffracted. The wavelengths contained in the beam will therefore be dispersed over a detector placed in the diffracted beam. To ensure that the diffraction from the crystal is not affected by the XFEL polarization, we have chosen the scattering plane of the crystal to orient vertically. This arrangement aligns the Bragg diffraction perpendicular to the scattering plane of the grating [see Fig 2(a)], effectively decoupling the crystal spectrometer dispersion from the dispersion of the beam splitter grating. The spectral range ΔE diffracted from the bent crystal spectrometer, of radius R, in relation to the x-ray beam width H [Fig. 2(b)], is given by [9]

$$\frac{\Delta E}{E} = \cot\theta_B \frac{H}{R\ \sin\theta_B}, \tag{2}$$

where E is the incoming beam energy and θ_B is the central Bragg diffraction angle.

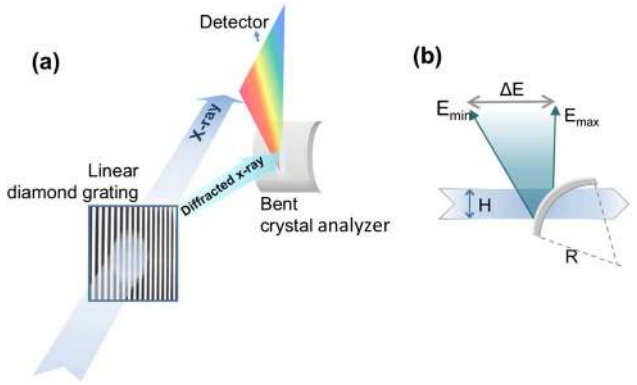

Fig. 2. (a) Schematic drawing of the experimental setup described in this Article. (b) Schematic drawing of the beam dispersion from the bent crystal.

A. Beam Splitter Grating

The diffraction grating was fabricated at the Laboratory for Micro and Nanotechnology at the Paul Scherrer Institut, Switzerland. A grating pitch of $d = 200$ nm was calculated from Eq. (1) to allow for sufficiently large Δy at a FEL beam wavelength λ in order to insert a spectrometer in the 1st-order diffraction beam without obstructing the direct beam. The grating pattern was defined on a ~10 μm thick diamond membrane using electron beam lithography, which was then transferred into the diamond membrane by reactive ion etching. This results in an all-diamond grating with a line depth of 1 μm, and a lateral size of 500 μm × 500 μm. Details of the fabrication processes can be found in [11].

The efficiency of the grating was measured prior to the LCLS experiment at the cSAXS beamline of the Swiss Light Source. At 6.2 keV photon energy, the diffracted +1st order beam contained ~1% of the incident beam intensity, an identical amount went to the −1st, and ~2% was absorbed by the diamond membrane. Higher diffraction orders are negligible, resulting in a 0th-order transmission of ~96%. As the diffraction efficiency and absorption both scale with the inverse square of the photon energy, we estimate that the zero-order transmission ranges from ~90% at 4 keV to ~98% at 8.4 keV photon energy.

B. Experiment

The spectrometer experiments were conducted at the XPP instrument at the LCLS [12] for several different photon energies ranging from 4.0 to 8.4 keV. All measurements with the XFEL, except for the ones at reduced pulse length (as discussed later in this Article), were performed at 40 fs average pulse duration and an average pulse energy of ~2 mJ. The beam size slit down to approximately $H \sim 400$ μm was accepted, and no monochromator or harmonic rejection mirrors were used throughout the measurements. The beam splitter grating was placed in a high-vacuum chamber approximately $D \sim 4$ m upstream of the spectrometer, leading to separations between the 1st- and 0th-order beams $\Delta y = 6.2 - 2.8$ mm for the above photon energies. The only alignment required for the grating was to center it to the XFEL beam, and no realignment was required during the experiments.

Figure 3(a) shows the transmitted direct beams and the diffracted negative and positive diffraction orders, imaged by using a YAG screen, a lens system, and an Adimec OPAL-1000 charge-coupled device (CCD) camera. During the measurements, the grating was extensively exposed to photon energies varying from 4.0 to 8.4 keV, at the full repetition rate of 120 Hz. We observed

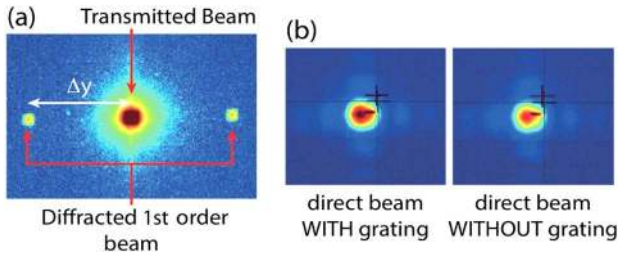

Fig. 3. Beam profiles recorded at 8.26 keV photon energy: (a) Beam profile at the crystal analyzer position. The separation of the 0th- and 1st-order diffraction beams is $\Delta y \sim 3$ mm. (b) Direct beam with the slits at ~200 m downstream of the spectrometer with and without the beam splitter grating in the beam.

no degradation of diffraction qualities of the grating throughout the entire duration of the experiment, confirming its radiation hardness. A further visual inspection at the end of the experiment also showed no change in the grating structure.

To investigate possible effects of the grating on the transmitted beam, we recorded the XFEL beam profile at ~200 m downstream of the XPP beamline [Fig. 3(b)], with the slits upstream of the grating closed down to 100 μm × 100 μm. No difference between the beam profiles recorded with and without the beam splitter grating in the beam was observed within the measurement sensitivity.

The setup consists of two bent crystal analyzer spectrometers, installed as follows: one in the diffracted 1st-order beam, and a second one in the transmitted 0th-order beam, in order to cross check the results for the same SASE pulses. The spectral resolution of both spectrometers is mainly determined by the chosen Bragg reflection, and their energy coverage ΔE is determined by Eq. (2). This ΔE should be equivalent to the XFEL bandwidth, which is reported to be around 0.5% FWHM [13]; this requires at least $\Delta E \sim 42$ eV at 8.4 keV to cover the FWHM range, or larger to capture the full spectra including their tails. We have therefore selected two scenarios: one that allows for a higher resolution with coverage just wide enough for the XFEL FWHM bandwidth, and a second that gives lower resolution but with broader spectral coverage.

The first scenario was realized by positioning a Si(111) crystal with $R = 78$ mm in the diffracted 1st-order beam, in order to achieve a high spectral resolution from the Si(333) reflection with $\Delta E \sim 60$ eV. The Si crystal was 10 μm thick, to allow for a small bending radius without affecting the attainable spectral resolution [9], with lateral dimensions of 5 mm × 10 mm. To achieve a uniform curvature, the crystal was glued onto the edge of a cylindrical plano–convex glass lens. The spectra from the Si(333) reflection were recorded with a 25 μm thick Ce:YAG screen, an imaging lens, and a high-speed camera (Hamamatsu ORCA Flash 4.0 V2) at 330 mm distance from the crystal surface. The total air-path for this 1st-order beam from the exit of the high-vacuum beamline to the YAG screen was ~550 mm. In the 0th-order beam, a Si(110) crystal with $R = 50$ mm was used to cover a wide range of $\Delta E > 300$ eV from the Si(220) reflection. The crystal was 10 μm thick with lateral dimensions of 5 mm × 15 mm, on a custom-designed aluminum mount. The signal from the Si(220) reflection was also monitored with a 100 μm thick YAG screen, a lens system, and an Adimec OPAL-1000 CCD camera at ~200 mm distance from the crystal, with total air-path of the beam of ~650 mm.

3. RESULT

The 2D spectrometer images and their projections from a typical single SASE pulse are shown in Fig. 4. The Si(333) Bragg angle at this photon energy range is close to 45°. For more than 60,000 recorded spectra, we observed the fluctuation of the SASE spectrum in bandwidth, intensity distribution, and central energy, as reported previously in [6,9,10], confirming the resolving capability of the setup.

The critical advantage of the beam splitting scheme is evident by the detailed spikes resolved from Si(333). The setup has proven that less than 1% of the original pulse energy is sufficient for spectral monitoring through air, while most of the pulse energy is left unaffected and hence available for experimental purposes—as demonstrated in [10], but with substantially better resolution. The spectrometer is in principle susceptible to spectral inhomogeneity, as reported in [14]. We have observed substantially less effect, and therefore minimal data treatment was required for the spectral profile mapping.

The minimum spike separation resolved from typical Si(333) spectra was 0.2–0.3 eV, corresponding to a resolving power of $E/\delta E > 3 \times 10^4$. The Si(333) reflection captured high-resolution and full range SASE spectra for over ~60%–70% of the shots, while some of the shots were only partially covered due to the energy jitter of the beam. In comparison, the Si(220) spectrometer was capable of monitoring the full ranges of the SASE spectra throughout, albeit with significantly lower resolution related to the increased Darwin width of the lower index reflection, as well as the smaller crystal–detector distance.

A detailed comparison of the two measurements can be obtained by matching the resolution of the spectra. The red curve in Fig. 4 shows the Si(333) spectrum artificially broadened by convolution with a Gaussian function of FWHM 0.5 eV. In the central energy range between 8359 and 8370 eV the Si(220) spectrum and the smoothened Si(333) spectrum match

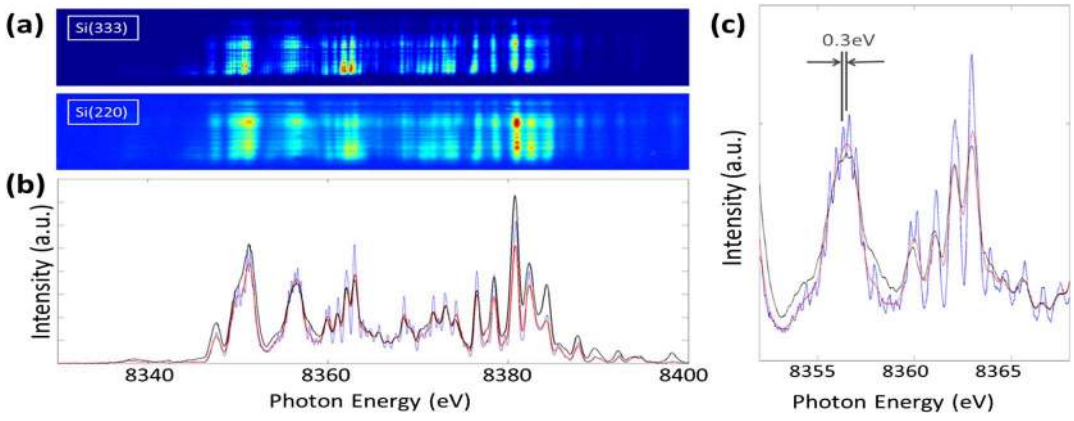

Fig. 4. (a) Typical single-shot spectra from the Si(333) and the Si(220) spectrometers. (b) Projections of the same shot from the Si(333) spectrometer (blue), the Si(333) spectrum after smoothening (red), and from the Si(220) spectrometer (black). The spectrum from the Si(220) reflection has similar overall features and intensity distribution, but the resolution is lower. (c) Detail of the same spectra. SASE spikes separated by ~0.3 eV were clearly resolved by the Si(333) spectrometer.

within 10% difference, and within 25% for a broader range between 8353 and 8377 eV. For energies outside of this central energy interval, the discrepancy is significantly larger, with the signal of the Si(333) spectrometer being systematically lower than that from its Si(220) counterpart. This effect is due to the intensity profile across the photon beam, such that these photon energies are Bragg-reflected by parts of the Si(333) spectrometer crystal that are illuminated by the upper and lower edges of the beam [see Fig. 2(b)] that have lower intensity than the center part of the beam. The Si(220) spectrometer maps the same energy range from the central, more homogeneous parts of the beam and, therefore, does not show the same decline in signal toward the edges of the spectrum. The influence of the beam intensity profile onto the measured spectra, including effects caused by the beam splitter's diffraction efficiency inhomogeneities, could be compensated by recording the −1st-order beam intensity profile and using it for normalization.

4. DISCUSSION

We also report additional results observed during the experiment, while varying the LCLS pulse duration from $\Delta t_R = 21$ fs to 12 and 8 fs FWHM, using the slotted foil method [1] and recording data from the Si(333) spectrometer at 8.38 keV. The pulse duration was monitored using the diagnostic data from the x-band transverse deflecting cavity (XTCAV) [15]. In first approximation, the spike width for Fourier-transform-limited pulses is related to the pulse duration by $\Delta E \cdot \Delta t_R = 1.82$ eV · fs [16]. The spectral widths that correspond to pulse lengths of $\Delta t_R =$ 21, 12, and 8 fs, according to the above relation, are $\Delta E =$ 0.087, 0.15, and 0.23 eV, respectively. Figure 5 shows the how the SASE spectra evolve as a function of the pulse duration.

The data in Fig. 5 show that, as the pulse duration is reduced, the spike width increases. To obtain a quantitative description of this phenomenon, the average spike FWHM was determined by fitting the spike profiles from several shots with Gaussian functions. After deconvolving the spectrometer resolution of ∼0.2 eV, we found average FWHM values of 0.22, 0.35, and 0.88 eV, for pulse lengths of 21, 12, and 8 fs, respectively. These values are significantly higher than what is reported above for Fourier-transform-limited pulses. This can be related to the presence of a pulse chirp. In this case, the bandwidth–pulse duration relation can be reformulated as $\Delta E \cdot \Delta t_R = 1.82 * \sqrt{(1 + \alpha^2)}$ (eV · fs), where α is a constant related to the pulse chirp [16]. We obtained $\alpha = 2.3$, 2.1, and 3.7 for pulse lengths of 21, 12, and 8 fs, respectively, indicating that not only are the measured SASE spike widths much wider than what is expected for Fourier-transform-limited pulses, but also that chirp parameter α varies for different pulse durations. Similar findings were reported in earlier works that measured the spike width directly by Gaussian fitting onto the spectra [7], or indirectly by electron bunch profile measurement [17]. Several possible causes for this spectral broadening were proposed; for example, it can be due to an energy chirp of the electron beam, electron bunch incoherence [18], or the pulse shortening method itself. The contributions from each process are indistinguishable from one another by judging from the spectra alone. However, combining this high-resolution spectral monitoring with electron bunch profile measurements [17] may provide additional insights into the underlying physics of the pulse shortening mechanisms, serving the purpose of accelerator optimization.

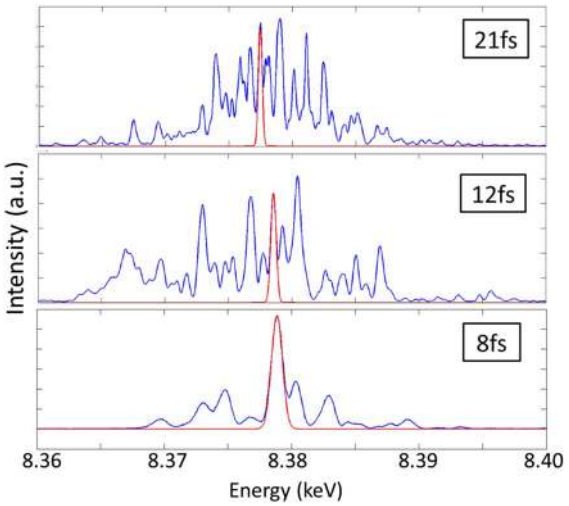

Fig. 5. Typical spectra obtained with the Si(333) spectrometer at 8.38 keV at various pulse lengths. The duration was controlled with the slotted foil method. Examples of a Gaussian fit (red) are shown for each spectrum to highlight that the spike width increases significantly with decreasing pulse length.

5. SUMMARY

In summary, we have demonstrated an *in situ* single-shot spectrometer setup for a multi-keV x-ray FEL that is nonintrusive, compact, and easy to align. The best resolved spectra showed $E/\delta E > 3 \times 10^4$ resolving power, using the Si(333) reflection, which was in good agreement with the spectra acquired simultaneously from the transmitted beam. The 1st-order diffraction beam was intense enough for on-line monitoring, allowing more than 90% of the beam energy for experiments. The diffraction grating withstood the full intensity of the LCLS XFEL beam at 4.0–8.4 keV and at full repetition rate of 120 Hz. We also confirmed that, within the selected x-ray energy range, the transmitted beam showed no obvious beam profile distortion and measurements require no replacement or realignment of the grating. Further investigation into the spectral profile changes with the pulse duration could be carried out in combination with the methods described in [7,16,17].

Funding. European Community's Seventh Framework Program (FP7/2007-2013) (290605, COFUND: PSI-FELLOW).

Acknowledgment. We thank Dr. S. Reiche and Dr. P. Costa for insightful advice and discussion. Si crystals were fabricated by Norcada Inc.

REFERENCES

1. P. Emma, K. Bane, M. Cornacchia, Z. Huang, H. Schlarb, G. Stupakov, and D. Walz, "Femtosecond and subfemtosecond x-ray pulses from a self-amplified spontaneous-emission-based free-electron laser," Phys. Rev. Lett. **92**, 074801 (2004).
2. E. L. Saldin, E. A. Schneidmiller, and M. V. Yurkov, "Statistical properties of the radiation from SASE FEL operating in the linear regime," Nucl. Instrum. Methods Phys. Res. A **407**, 291 (1998).
3. P. N. Juranić, M. Martins, J. Viefhaus, S. Bonfigt, L. Jahn, M. Ilchen, S. Klumpp, and K. Tiedtke, "Using I-TOF spectrometry to measure photon energies at FELs," J. Instrum. **4**, P09011 (2009).

4. W. F. Schlotter, J. J. Turner, M. Rowen, P. Heimann, M. Holmes, O. Krupin, M. Messerschmidt, S. Moeller, J. Krzywinski, R. Soufli, M. Fernández-Perea, N. Kelez, S. Lee, R. Coffee, G. Hays, M. Beye, N. Gerken, F. Sorgenfrei, S. Hau-Riege, L. Juha, J. Chalupský, V. Hájková, A. P. Mancuso, A. Singer, O. Yefanov, I. A. Vartanyants, G. Cadenazzi, B. Abbey, K. A. Nugent, H. Sinn, J. Lüning, S. Schaffert, S. Eisebitt, W. S. Lee, A. Scherz, A. R. Nilsson, and W. Wurth, "The soft x-ray instrument for materials studies at the linac coherent light source x-ray free-electron laser,"Rev. Sci. Instrum. **83**, 043107 (2012).
5. P. Heimann, O. Krupin, W. F. Schlotter, J. Turner, J. Krzywinski, F. Sorgenfrei, M. Messerschmidt, D. Bernstein, J. Chalupský, V. Hájková, S. Hau-Riege, M. Holmes, L. Juha, N. Kelez, J. Lüning, D. Nordlund, M. F. Perea, A. Scherz, R. Soufli, W. Wurth, and M. Rowen, "Linac coherent light source soft x-ray materials science instrument optical design and monochromator commissioning," Rev. Sci. Instrum. **82**, 093104 (2011).
6. M. Yabashi, J. Hastings, M. S. Zolotorev, H. Mimura, H. Yumoto, S. Matsuyama, K. Yamauchi, and T. Ishikawa, "Single-shot spectrometry for x-ray free-electron lasers," Phys. Rev. Lett. **97**, 084802 (2006).
7. Y. Inubushi, K. Tono, T. Togashi, T. Sato, T. Hatsui, T. Kameshima, K. Togawa, T. Hara, T. Tanaka, H. Tanaka, T. Ishikawa, and M. Yabashi, "Determination of the pulse duration of an x-ray free electron laser using highly resolved single-shot spectra," Phys. Rev. Lett. **109**, 144801 (2012).
8. T. Katayama, Y. Inubushi, Y. Obara, T. Sato, T. Togashi, K. Tono, T. Hatsui, T. Kameshima, A. Bhattacharya, Y. Ogi, N. Kurahashi, K. Misawa, T. Suzuki, and M. Yabashi, "Femtosecond x-ray absorption spectroscopy with hard x-ray free electron laser,"Appl. Phys. Lett. **103**, 131105 (2013).
9. D. Zhu, M. Cammarata, J. M. Feldkamp, D. M. Fritz, J. B. Hastings, S. Lee, H. T. Lemke, A. Robert, J. L. Turner, and Y. Feng, "A single-shot transmissive spectrometer for hard x-ray free electron lasers," Appl. Phys. Lett. **101**, 034103 (2012).
10. P. Karvinen, S. Rutishauser, A. Mozzanica, D. Greiffenberg, P. N. Juranić, A. Menzel, A. Lutman, J. Krzywinski, D. M. Fritz, H. T. Lemke, M. Cammarata, and C. David, "Single-shot analysis of hard x-ray laser radiation using a noninvasive grating spectrometer," Opt. Lett. **37**, 5073 (2012).
11. C. David, S. Gorelick, S. Rutishauser, J. Krzywinski, J. Vila-Comamala, V. A. Guzenko, O. Bunk, E. Färm, M. Ritala, M. Cammarata, D. M. Fritz, R. Barrett, L. Samoylova, J. Grünert, and H. Sinn, "Nanofocusing of hard x-ray free electron laser pulses using diamond based Fresnel zone plates," Sci. Rep. **1**, 57 (2011).
12. R. Alonso-Mori, D. Sokaras, D. Zhu, T. Kroll, M. Chollet, Y. Feng, J. M. Glownia, J. Kern, H. T. Lemke, D. Nordlund, A. Robert, M. Sikorski, S. Song, T. Weng, and U. Bergmann, "Photon-in photon-out hard x-ray spectroscopy at the Linac Coherent Light Source," J. Synchrotron Radiat. **22**, 612 (2015).
13. P. Emma, R. Akre, J. Arthur, R. Bionta, C. Bostedt, J. Bozek, A. Brachmann, P. Bucksbaum, R. Coffee, F.-J. Decker, Y. Ding, D. Dowell, S. Edstrom, A. Fisher, J. Frisch, S. Gilevich, J. Hasting, G. Hays, P. Hering, Z. Huang, R. Iverson, H. Loos, M. Messerschmidt, A. Miahnahri, S. Moeller, H.-D. Nuhn, G. Pile, D. Ratner, J. Rzepiela, D. Schultz, T. Smith, P. Stefan, H. Tompkins, J. Turner, J. Welch, W. White, J. Wu, G. Yocky, and J. Galayda, "First lasing and operation of an Ångstrom-wavelength free-electron laser," Nat. Photonics **4**, 641 (2010).
14. D. Zhu, M. Cammarata, J. Feldkamp, D. M. Fritz, J. Hastings, S. Lee, H. T. Lemke, A. Robert, J. Turner, and Y. Feng, "Design and operation of a hard x-ray transmissive single-shot spectrometer at LCLS," J. Phys. Conf. Ser. **425**, 052033 (2013).
15. A. Y. Murokh, R. B. Agustsson, S. Boucher, P. Frigola, D. Alesini, R. J. England, J. B. Rosenzweig, J. England, G. Travish, and V. Yakimenko, "Design and fabrication of an x-band traveling wave deflection mode cavity for longitudinal characterization of ultra-short electron beam pulses," in *Proceedings of European Particle Accelerator Conference*, Genoa, Italy (2008).
16. J.-C. Diels and W. Rudolph, *Ultrashort Laser Pulse Phenomena* (Academic, 2006), p. 10.
17. J. Wu, Y. Ding, P. Emma, Z. Huang, H. Loos, M. Messerschmidt, E. Schneidmiller, and M. Yurkov, "LCLS x-ray pulse duration measurement using the statistical fluctuation method," in *Proceedings of the 2010 Free-Electron Laser Conference*, Malmö, Sweden (2010).
18. A. A. Lutman, Y. Ding, Y. Feng, Z. Huang, M. Messerschmidt, J. Wu, and J. Krzywinski, "Femtosecond x-ray free electron laser pulse duration measurement from spectral correlation function," Phys. Rev. Spec. Top. Accel. Beams **15**, 030705 (2012).